Supplementary Information

Run-Tumble Like Motion of a Camphor-Infused Marangoni Swimmer

February 8, 2025

1 Image Analysis Techniques

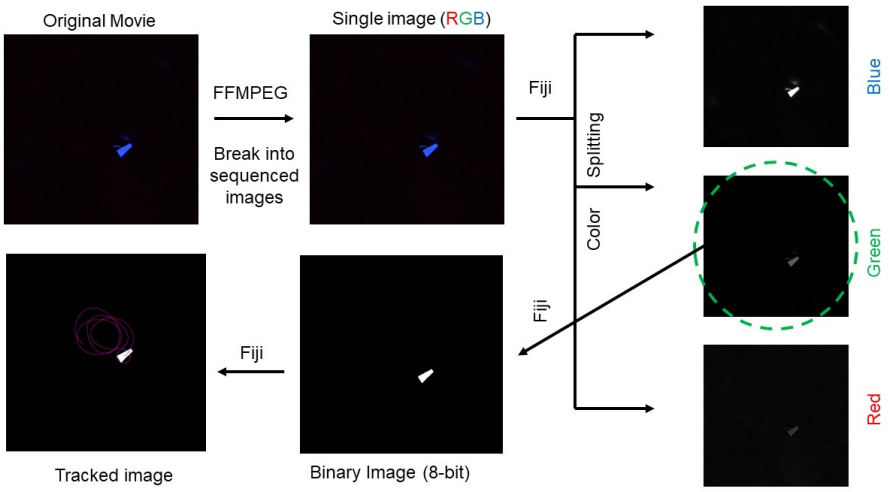

SF 1: Schematic representation of the way of image processing

Fiji and FFMPEG were used as resources in our image analysis process. FFMPEG facilitated the conversion of video files into a series of successive images, which were subsequently put into Fiji. The processed images were then subjected to particle tracking, resulting in the center of mass (x_c, y_c) data extraction. Two Fiji plugins helped us track precisely (Plugin - Trackmate) and measure the swimmer's orientation (Plugin - OrientatioJ) within the images. The above schematic (SF 1) represents the way followed to pre-process the experimental videos. The green color channel was picked up to get a better contrast when it was converted into a binary image. Thereafter, the data was analyzed using Python code, with the help of widely recognized functions like 'peak finder', 'peak width', and 'Savgol filter', which were used to characterize the data.

2 Why hasn't the petri dish been used in the experiments?

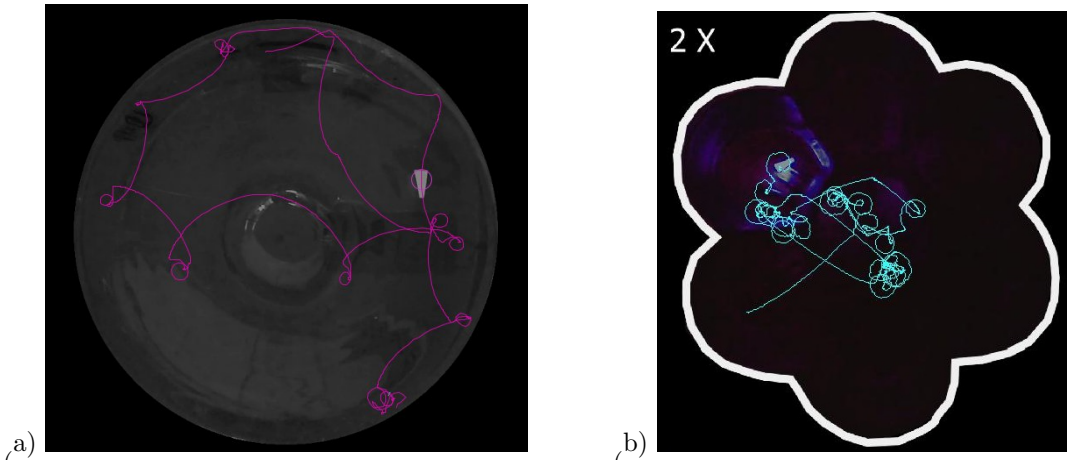

SF 2: Traced path of the swimmer within (a) a petri dish and (b) a flowered shape container.

Previously, several experiments (8-9 Experiments) were conducted using a round-shaped Petri dish (diameter $\approx$ 270 mm) in which the trapezoidal-shaped swimmer stuck to the boundary and began moving along it due to the meniscus effect. The formation of a concave meniscus between the wall of the Petri dish and the water surface contributed to the swimmer becoming stuck in the periphery. A similar-sized flower-shaped container was employed to address this boundary effect. This type of container is commonly used to reduce the boundary effect and helps to inject the swimmer into the middle by producing an inward flux. If the swimmer's activity is higher, it has a greater chance of moving into the middle; otherwise, this effect may not be as prominent. The above (SF 2) and Movies S2 and S5 show the difference in motion between the flower-shaped container and the Petri dish.

3 Different shapes have been made, but why has this specific shape been chosen?

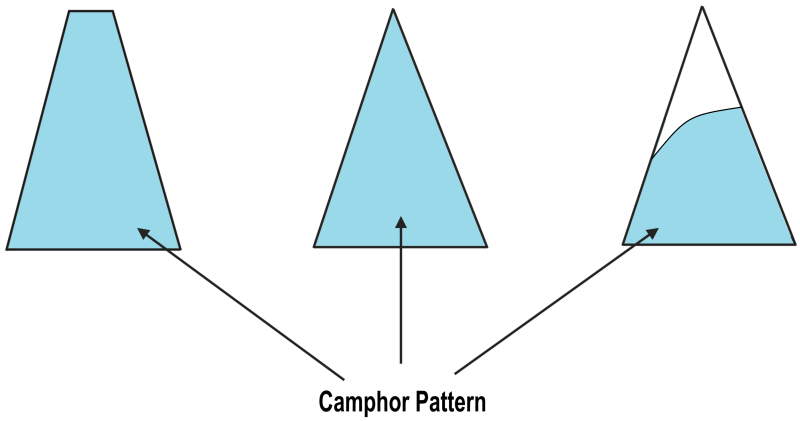

SF 3: Different-shaped Marangoni swimmers

Various experiments were conducted using different shapes (SF 3) for the Marangoni swimmer, including those using the Petri dish. However, none of these shapes featured distinct camphor patterns that could demonstrate the 'run' and 'tumble' motion. SF 4 illustrates the trapezoidal shape with a camphor gradient, which resulted in the observation of all three states. In contrast, only running or tumbling

were observed in other shapes. Additional shapes may be designed to produce this characteristic motion. As of now, only the trapezoidal shape has demonstrated this behavior. One possible explanation for the appearance of the three states in SF 4 could be the presence of a gradient in the camphor pattern, which generates two dominant forces: one responsible for the straight run and the other for producing torque. The force that will dominate at any given moment is unpredictable. These two forces are generated exclusively due to local surface tension gradients.

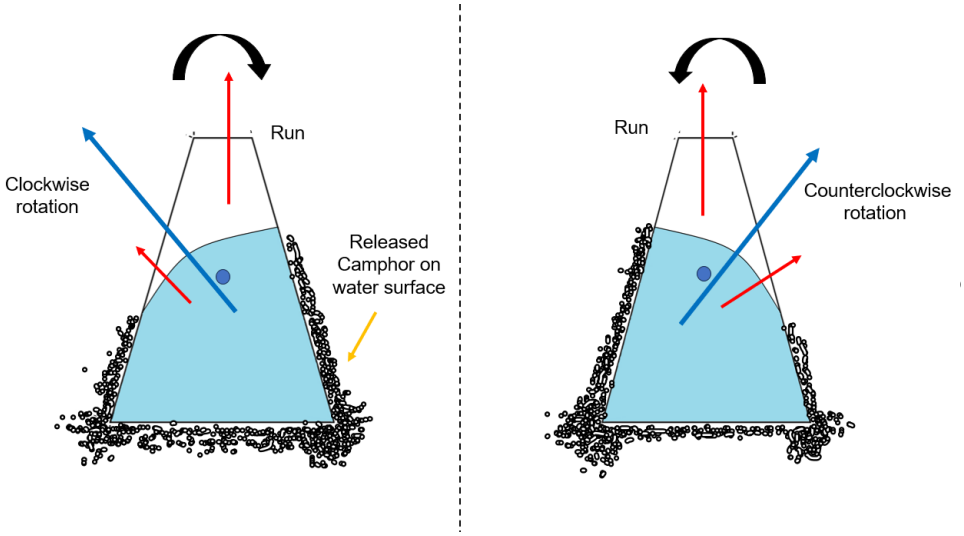

SF 4: Schematic representation of two different camphor patterns and the rotational directions. One is the mirror reflection of the other one.

4 Orientation with respect to time

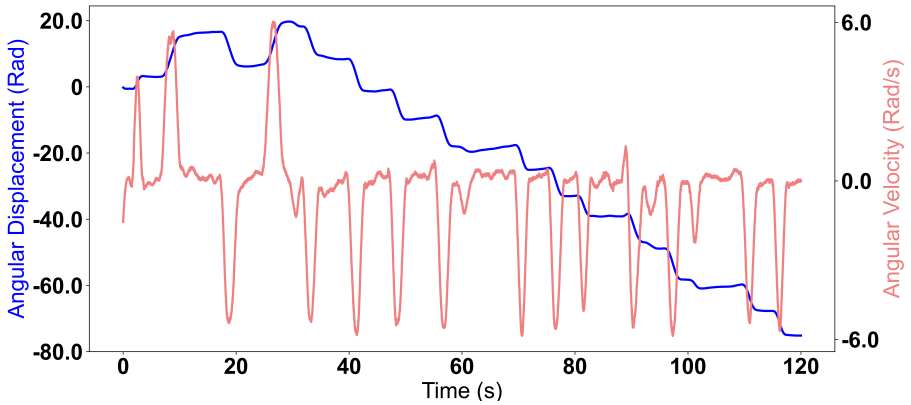

SF 5: The left-hand y-axis shows the time series of angle (Radian), and the right-hand y-axis displays the angular velocity (Rad/s) of Movie S1.

All analyses were conducted using the Marangoni swimmer, illustrated in the left part of SF 4. It is characterized by a shape that primarily produces clockwise rotation (tumble), 'run', and 'rest' states. SF 5 demonstrates that the angular velocity is negative only in the case of clockwise rotation; for counterclockwise rotation, it is the opposite. When there is no change in angular displacement, the swimmer is either at 'rest' or performing a 'run' in a specific direction without any change in orientation. If it sometimes shows a counterclockwise rotation, the force arises from the top part of the center of mass because the system is stochastic. Movie S4 shows that the counterclockwise rotation is more frequent for the other camphor pattern. SF 6 shows the statistics of taking clockwise and counterclockwise rotations depending on the camphor pattern on the swimmer.

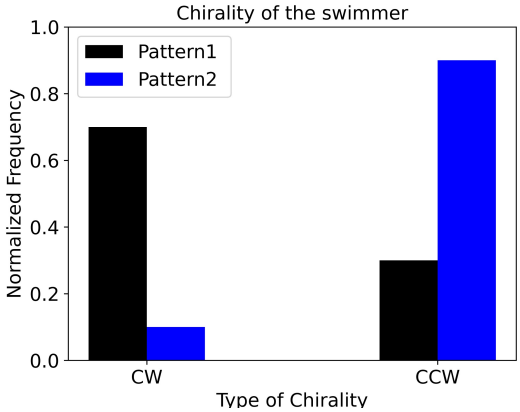

SF 6: Clockwise and Counterclockwise rotation depend on the specific pattern of the camphor profile SF 4. Data has been taken from the experiments Movie S4.

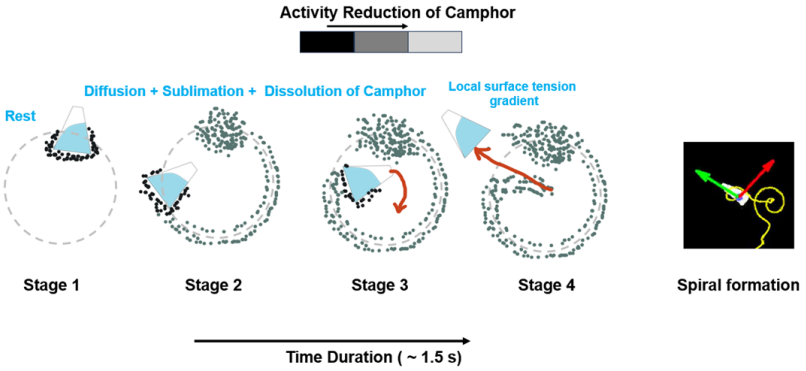

SF 7: Schematic representation for the formation of spiral trajectory at the tumbling

Hence, SF 7 gives an intuitive explanation for the formation of a spiral trajectory. It releases a large amount of camphor during resting, and thereafter, it avoids that path because motion always happens from low to high surface tension.

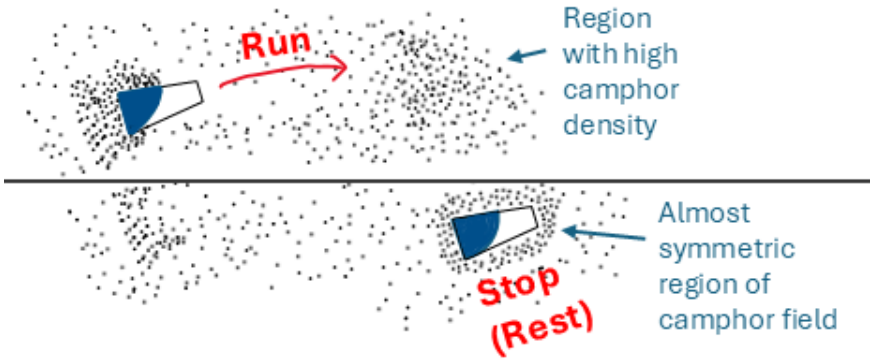

SF 8: Schematic representation of the distributed camphor profile. And how it influences the motion of the swimmer.

5 Numerical Model

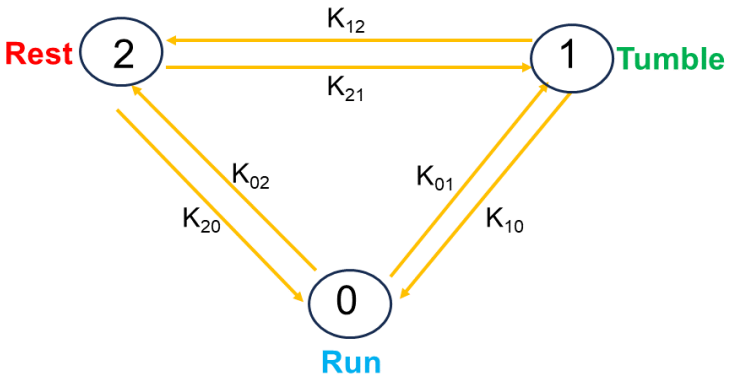

SF 9: Schematic representation of the transitions from one state to another with specific transition rates (s^{-1}). Here, transitions occur in both ways ($0 \leftrightarrow 1 \leftrightarrow 2 \leftrightarrow 0$).

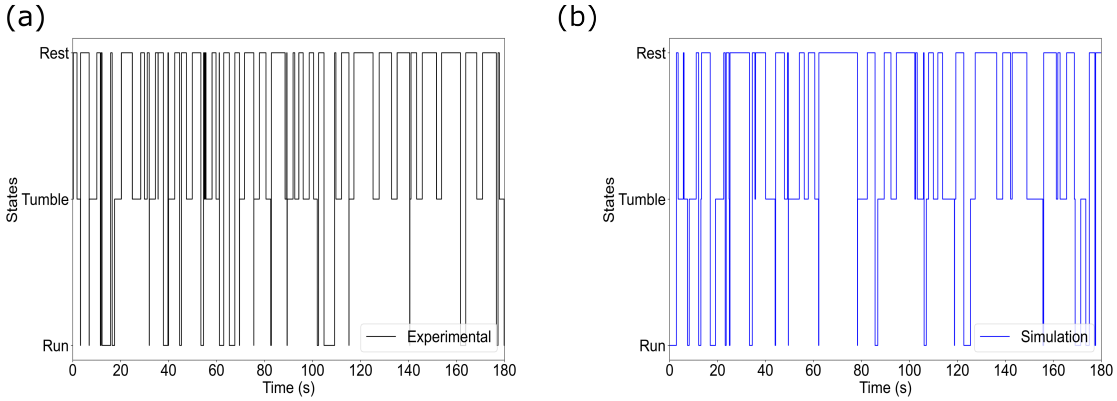

SF 10: Change of three states over time. From (a) experiment, (b) simulation (both-way transition). In the simulation, we consider the both-way transitions with specific rates (s^{-1}): 'Run' $\leftrightarrow$ 'Tumble' $\leftrightarrow$ 'Rest' $\leftrightarrow$ 'Run'.

This study proposes a simple model that effectively describes the statistical behavior of the system (Eq. 1 - 4). The system comprises three states: 'run', 'tumble', and 'rest'. The schematic (SF 9) illustrates the transitions between states of the system, characterized by specific transition rates, $k_{01}, k_{02}, k_{10}, k_{12}, k_{20}, k_{21}$ (s^{-1}). The empirical values of these rates are derived solely from experimental data (Table 1). The mean durations for each state are as follows: $t_{run}(\ 1.1s), t_{tumble}(\ 1.97s), t_{rest}(\ 3.0s)$. The result is similar with the single-way transitions also, but we consider the both-way transitions to make the model more realistic. It infers that the residential times of each state are important to explain the system qualitatively.

Transition probabilities	Transition rates (s^{-1})	Estimated values (s^{-1})
$p_{01} = 0.5154$	$k_{01} = p_{01} \times \frac{1}{t_{run}}$	0.3946
$p_{02} = 0.4845$	$k_{02} = p_{02} \times \frac{1}{t_{run}}$	0.3727
$p_{10} = 0.2387$	$k_{10} = p_{10} \times \frac{1}{t_{tumble}}$	0.1212
$p_{12} = 0.7613$	$k_{12} = p_{12} \times \frac{1}{t_{tumble}}$	0.3864
$p_{20} = 0.3674$	$k_{20} = p_{20} \times \frac{1}{t_{rest}}$	0.1224
$p_{21} = 0.6325$	$k_{21} = p_{21} \times \frac{1}{t_{rest}}$	0.2275

Table 1: Table of Transition Rates and Probabilities (From Experiments)

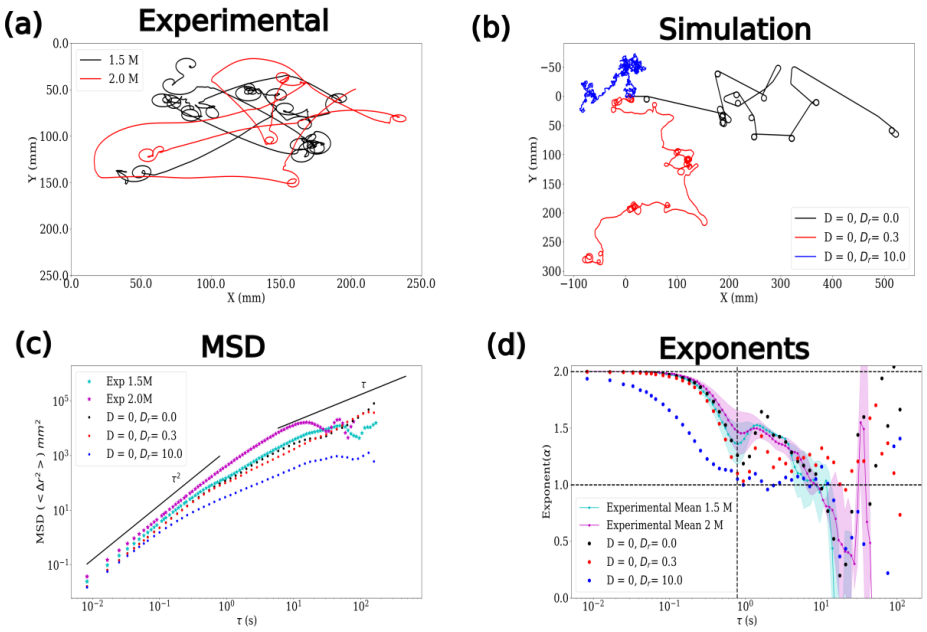

SF 11: The trajectory of the swimmer from (a) experimental (1.5 M), (b) simulation. In simulation, $v_0 = 20.0$ mm/s, $\Omega_0 = 4.0$ rad/s, $D = 0.0\ mm^2/s$, $D_r = 0.3\ rad^2/s$, $\lambda = 0.3$

In this model, the swimmer has been represented as a point particle. The center of mass coordinates $(x(t), y(t))$ and the orientation $(\theta(t))$ of the swimmer adhere to the Langevin equations in the overdamped limit. The proposed equations are presented below. The $\zeta_x(t)$, $\zeta_y(t)$, and $\zeta_\theta(t)$ represent delta-correlated Gaussian white noises within the system. The state function $\sigma(t)$ has been generated utilizing the Gillespie algorithm. In this algorithm, all transition rates are derived from experimental data (Table 1).

$$\dot{x}(t) = v_0\Theta(\frac{3}{2} - \sigma(t))(1 - \lambda\sigma(t))\cos\theta(t) + \sqrt{2D}\zeta_x(t) \tag{1}$$

$$\dot{y}(t) = v_0\Theta(\frac{3}{2} - \sigma(t))(1 - \lambda\sigma(t))\sin\theta(t) + \sqrt{2D}\zeta_y(t) \tag{2}$$

$$\dot{\theta}(t) = \Omega_0\Theta(\frac{3}{2} - \sigma(t))\sigma(t) + \sqrt{2D_r}\zeta_\theta(t) \tag{3}$$

$$\sigma(t) = \begin{cases} 0, & \text{run} \\ 1, & \text{tumble} \\ 2, & \text{rest} \end{cases} \tag{4}$$

Parameters	Range of the value (From Experiment)	Used value in the Numerical Model
Diffusion Coefficient (D)	$---$	0.0 $\frac{mm^2}{s}$
Rotational Diffusion Coefficient (D_r)	$< \frac{2\Omega_0}{3\pi}\ \frac{rad^2}{s}$	0.3 $\frac{rad^2}{s}$
run Speed (v_0)	$15 - 45\ \frac{mm}{s}$	20.0 $\frac{mm}{s}$
tumble Speed (Ω_0)	$1.2 - 4.8\ \frac{rad}{s}$	4.0 $\frac{rad}{s}$
Radius of Tumbling (R_0)	$2.0 - 14.5\ mm$	3.5 mm
free Parameter (λ)	$0.1 - 0.6$	0.3
Transition rates (k_{01}, k_{12}, k_{20}, k_{10}, k_{20}, k_{21})	0.3946, 0.3727, 0.1212, 0.3864, 0.1224, 0.2275 s^{-1}	0.3946, 0.3727, 0.1212, 0.3864, 0.1224, 0.2275 s^{-1}

Table 2: Table of parameters used in the Model (From Experimental Data).

All the parameters utilized in this model are derived exclusively from the experimental data. SF 12 and 13 illustrate the range of the translational and angular speeds, as well as the radius of tumbling. These

three parameters enable the estimation of the range of the nondimensional tuning parameter (λ, Table 2). Consequently, the model yields good results (MSD and MSAD) that correspond closely with the experimental findings (SF 11 and 17).

To analyze the behavior of the system for the individual state, the conditions for three states were applied, and equations 1 - 3 were solved, disregarding the noise terms. Consequently, equations 13 and 23 demonstrate the expression of the Mean Square Displacement (MSD) for that specific state. In the 'tumble' state, the MSD exhibits oscillatory behavior. From SF 11 MSD, it can be observed that the system initially demonstrates ballistic motion; subsequently, the tumbling and rest states dominate in the system. The dip in the exponent($\alpha(\tau)$) arises at the time scale $\frac{3\pi}{2\Omega_0}$ (SF 10) when the system show purely rotational motion. Additionally, SF 5, 6, 10, and 13 indicate that the rotational and translational diffusion coefficients (D_r, D) are notably low in this system due to the observed ballistic motion in Mean Square Angular Displacement (MSAD) ($< \Delta\theta)^2 >$) and in Mean Square Displacement (MSD). These equations suggest that the swimmer rotates predominantly in a clockwise direction with a constant angular velocity for this specific pattern of the swimmer (SF 4 left part). Also, it is interesting to note that the trajectory of the experimental data matches the simulation for the low rotational diffusion coefficient extremely well.

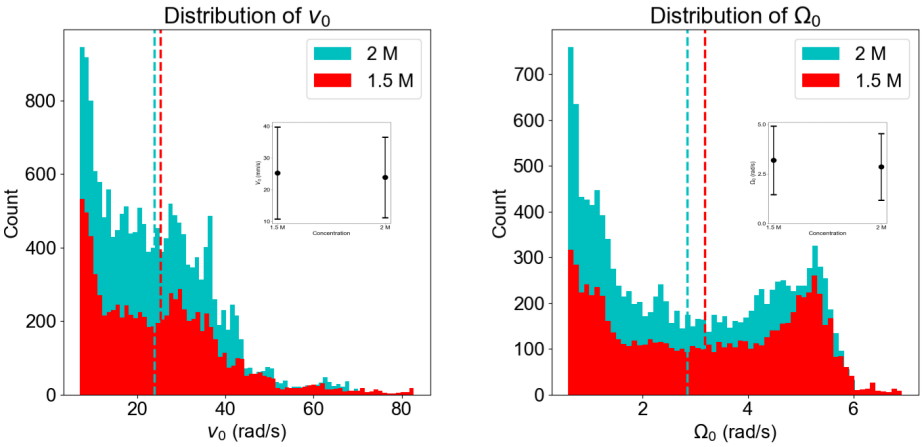

SF 12: Estimation of the mean speeds of the swimmer from experiments (1.5 M and 2 M). $v_0 = 25.28 \pm 14.49$ mm/s (1.5 M) and 23.88 ± 12.7 (2 M). $\Omega_0 = 3.186 \pm 1.726$ rad/s (1.5 M) and 2.856 ± 1.68 (2 M) rad/s.

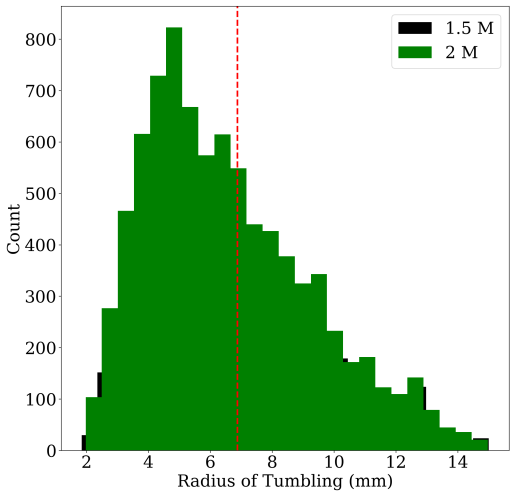

SF 13: Estimation of the mean tumbling radius of the swimmer from experiments (1.5 M and 2 M). $R_0 = 6.864(6.591) \pm 2.752(2.673)$ mm for 1.5 M (2.0 M).

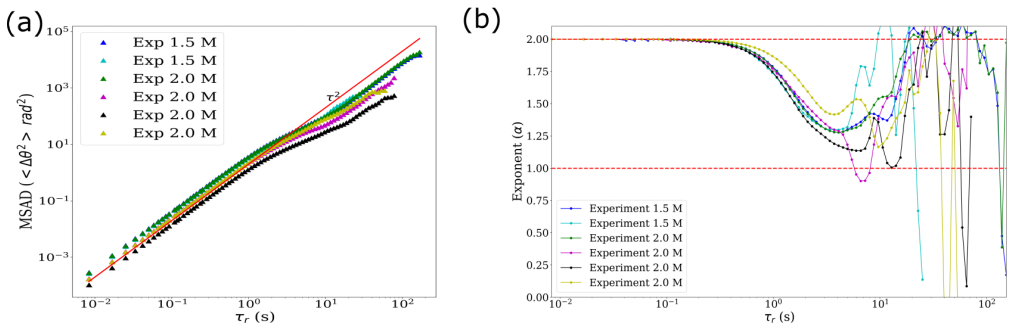

SF 14: (a) Mean squared angular displacement (MSAD), (b) exponents of the MSAD.

If one considers $\sigma = 0$, which corresponds to the 'run' state and neglects the strength of the random white noise, the Eq. (1)-(3) will be,

$$\dot{x}(t) = v_0 \cos\theta(t) \tag{5}$$

$$\dot{y}(t) = v_0 \sin\theta(t) \tag{6}$$

$$\dot{\theta}(t) = 0 \tag{7}$$

$$x(t) = v_0 t \cos\theta_0 + x_0 \tag{8}$$

$$y(t) = v_0 t \sin\theta_0 + y_0 \tag{9}$$

$$\theta(t) = \theta_0 \tag{10}$$

$$x(t+\tau) - x(t) = v_0 \tau \cos\theta_0 \tag{11}$$

$$y(t+\tau) - y(t) = v_0 \tau \sin\theta_0 \tag{12}$$

Hence, the MSD will be,

$$< (x(t+\tau) - x(t))^2 >_t + < (y(t+\tau) - y(t))^2 >_t = v_0^2 \tau^2 \tag{13}$$

If one considers $\sigma = 1$, which corresponds to the 'tumble' state and neglects the strength of the random white noise, the Eq. (1)-(3) will be,

$$\dot{x}(t) = v_0 \cos\theta(t)(1-\lambda) \tag{14}$$

$$\dot{y}(t) = v_0 \sin\theta(t)(1-\lambda) \tag{15}$$

$$\dot{\theta}(t) = \Omega_0 \tag{16}$$

$$x(t) = \frac{v_0}{\Omega_0}(1-\lambda)\sin(\Omega_0 t + \theta_0) + x_0 \tag{17}$$

$$y(t) = -\frac{v_0}{\Omega_0}(1-\lambda)\cos(\Omega_0 t + \theta_0) + y_0 \tag{18}$$

$$\theta(t) = \Omega_0 t + \theta_0 \tag{19}$$

$$x(t+\tau) - x(t) = \frac{v_0}{\Omega_0}(1-\lambda)(\sin(\Omega_0(t+\tau)) - \sin(\Omega_0(t))) \tag{20}$$

$$y(t+\tau) - y(t) = -\frac{v_0}{\Omega_0}(1-\lambda)(\cos(\Omega_0(t+\tau)) - \cos(\Omega_0(t))) \tag{21}$$

Hence, the MSD will be,

$$< (x(t+\tau) - x(t))^2 >_t + < (y(t+\tau) - y(t))^2 >_t = 4\frac{v_0^2}{\Omega_0^2}(1-\lambda)^2(\sin(\frac{\Omega_0\tau}{2}))^2 \tag{22}$$

$$< (x(t+\tau) - x(t))^2 >_t + < (y(t+\tau) - y(t))^2 >_t = 2\frac{v_0^2}{\Omega_0^2}(1-\lambda)^2(1-\cos(\Omega_0\tau)) \tag{23}$$

If we find the exponent $(\alpha(\tau))$ of eq.(23),

$$\alpha(\tau) = \frac{d(MSD(\tau))}{d\tau} = 2\frac{v_0^2}{\Omega_0}(1-\lambda)^2\sin(\Omega_0\tau) \tag{24}$$

The minima of eq.(24) come at $\tau = \frac{3\pi}{2\Omega_0}$ which is the time scale for the system that exhibits tumbling dynamics exclusively.

After Taylor expansion of $(1-\cos(\Omega_0\tau))$, the eq.(23) will be,

$$< (x(t+\tau) - x(t))^2 >_t + < (y(t+\tau) - y(t))^2 >_t = 2\frac{v_0^2}{\Omega_0^2}(1-\lambda)^2(1-(1-\frac{\Omega_0^2\tau^2}{2}+\frac{\Omega_0^4\tau^4}{24}-...)) \tag{25}$$

$$< (x(t+\tau) - x(t))^2 >_t + < (y(t+\tau) - y(t))^2 >_t = 2\frac{v_0^2}{\Omega_0^2}(1-\lambda)^2(\frac{\Omega_0^2\tau^2}{2}-\frac{\Omega_0^4\tau^4}{24}+...) \tag{26}$$

If one considers $\sigma = 2$, which corresponds to the 'rest' state and neglects the strength of the random white noise, the Eq. (1) - (3) will be,

$$\dot{x}(t) = 0 \tag{27}$$

$$\dot{y}(t) = 0 \tag{28}$$

$$\dot{\theta}(t) = 0 \tag{29}$$

$$x(t) = x_0 \tag{30}$$

$$y(t) = y_0 \tag{31}$$

$$\theta(t) = \theta_0 \tag{32}$$

The swimmer stays at the same location (x_0, y_0) and points in the same direction (θ_0). It does not exhibit any motion.

6 Effect in Motion Due to Boundary

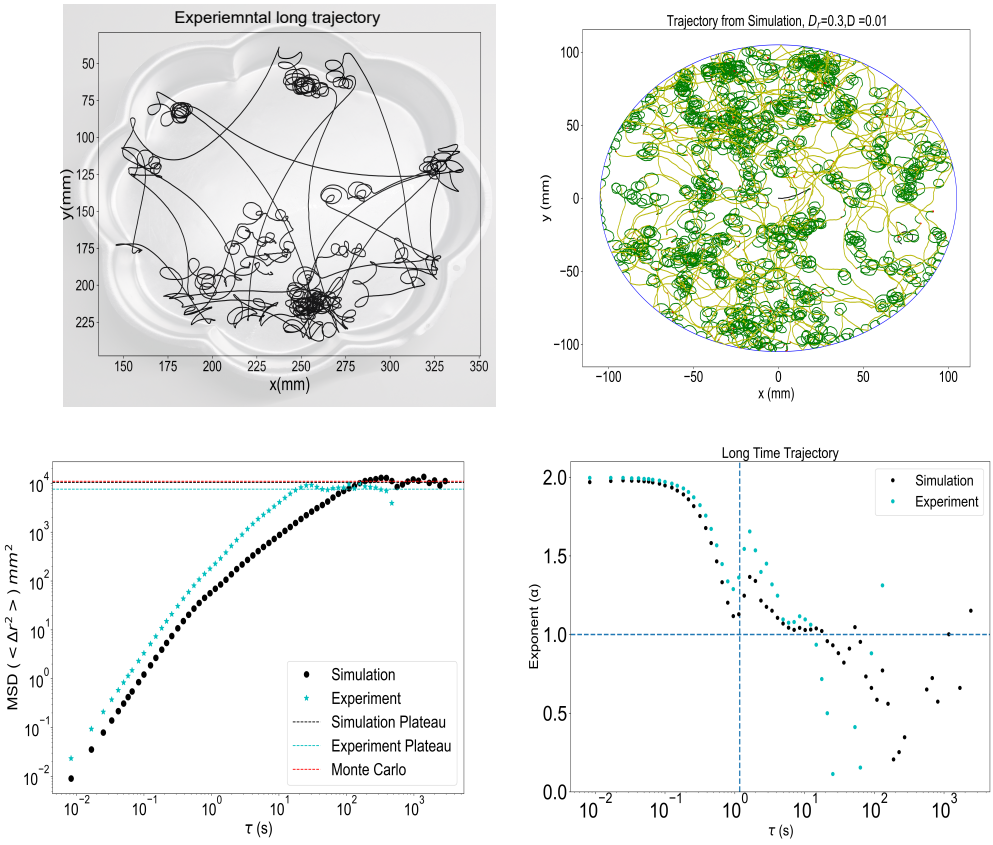

SF 15: Top left: trajectory of the swimmer within a gentle flower shaped container. Top right: trajectory from the simulation considering the boundary effect. Bottom left: MSD comparison. Bottom right: exponent comparison

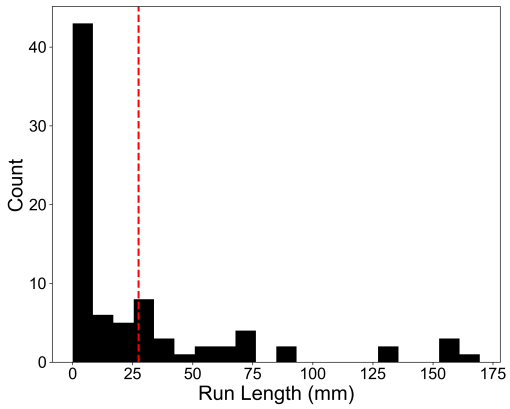

SF 16: The run length distribution of the Marangoni swimmer. The mean run length is 27.51 mm. Experiment has been conducted within a gentle flower shaped container.

Additional Experimental Movies

The frame rate of movies S2-S6 was 120/s and S7-S8 was 60/s. The experiments were conducted in UV light to obtain better contrast, which helped in image analysis.

Movie S1: It shows the dynamics of a swimmer having a concentration of 1.5 M (after image processing). The red and green arrows show the velocity and orientation vectors, respectively. The yellow-colored

path is the corresponding trajectory.

Movie S2: An experimental movie about a swimmer with a concentration of 1.5 M without image processing.

Movie S3: An experimental movie about a swimmer with a concentration of 2.0 M without image processing.

Movie S4: Experimental movie of a swimmer having a concentration of 2.0 M without image processing, but with the mirror image of the camphor pattern (Right part of the SF 4).

Movie S5: Experimental movie of a swimmer with a concentration of 1.5 M without image processing within a Petri Dish (Diameter $\approx$ 270 mm), but this experiment was performed in normal light.

Movie S6: Experimental movie of a swimmer with a concentration of 2.0 M without image processing within a Flower-shaped container without ridges (Diameter $\approx$ 220 mm).

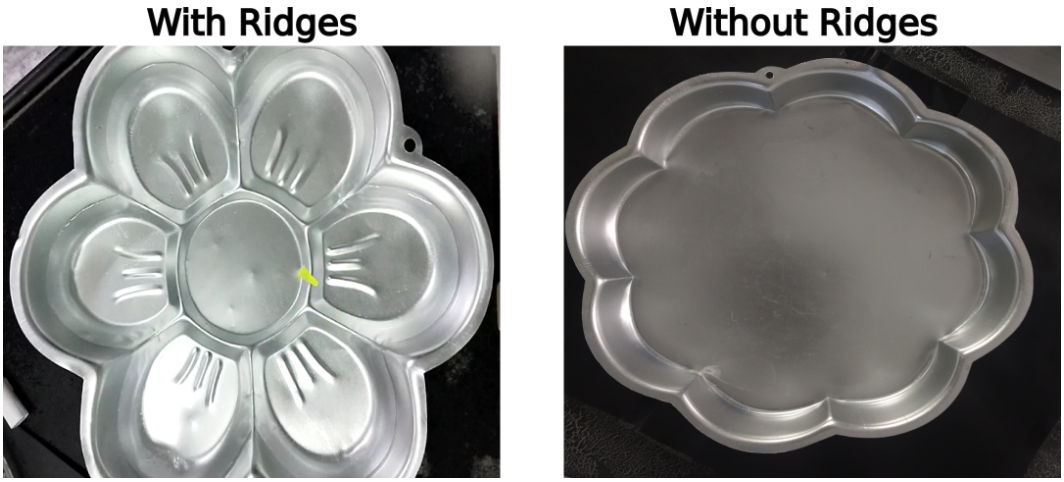

SF 17: Experiments have been verified with the flower-shaped container (a) with ridges and (b) without ridges.

Movie S7: Small portion of the experiment using 7-Hydroxycoumarin to visualize the camphor trail.

Movie S8: Experimental movie of a swimmer which is completely filled with camphor of 2.0 M without image processing within a Flower-shaped container without ridges (Diameter $\approx$ 220 mm).